Journal of
Mechanics of
Materials and Structures

ENERGY-MINIMIZING OPENINGS AROUND A FIXED HOLE IN AN ELASTIC PLATE

Shmuel Vigdergauz

Volume 5, No. 4 April 2010

mathematical sciences publishers

JOURNAL OF MECHANICS OF MATERIALS AND STRUCTURES
Vol. 5, No. 4, 2010

ENERGY-MINIMIZING OPENINGS AROUND A FIXED HOLE IN AN ELASTIC PLATE

SHMUEL VIGDERGAUZ

The design of elastic structures to optimize the stress state of flat plates with appropriately shaped construction holes is a problem of considerable mathematical and industrial significance. This paper continues the shape optimization study previously reported in this journal, **1**:2 (2006), 307–406, for the energy-minimizing single hole under remote shear, and in **3**:7 (2008), 1341–1363 for two identical holes. Here, a challenging and more practical three-hole arrangement is considered, where the central hole is fixed, while the two identical side holes are varied not only in their shapes, but also in their areas.

This twofold novelty is resolved by enhancing a standard genetic algorithm combined with a general method of shape parametrization for multiconnected regions. The method employs conformal mapping of the outside of each optimized contour *separately* onto the outside of a unit circle, as was first proposed in the 2008 paper. We show here that this approach has a significant computational advantage over the common practice of mapping the entire domain under consideration. The numerical simulations present in detail the influence of sizes, shapes, and relative positions of the openings on the induced energy increment and, to a much smaller extent, on the local stresses. The main result is that, compared to a single hole, interacting optimal openings induce up to 15%–19% less energy, depending on the hole spacing and the central hole shape.

1. Introduction

In spite of intensive studies carried out over the last decades, the problem of diminishing the weakening effect of construction holes in a flat elastic plate remains an object of much attention in engineering the optimal design. Various strengthening technologies, such as auxiliary unloading holes, reinforcement rings, and others are known so far, each posing its own elastostatic problem. Of particular assistance here is proper shaping of holes, which may significantly improve the stress-strain state of perforated plates. This optimization scheme is all the more promising, as the hole area is usually of much more importance than its shape, which thus permits a certain design freedom.

In modelling the problem, the plate is infinite and linearly elastic. Furthermore, although the engineering ideal is to minimize the maximum hoop stress occurring along the holes' boundaries, we choose here the weaker and numerically easier integral criterion of the energy increment brought by the holes in the uniform stress state of an undamaged plate under the same load. Besides computational convenience, this choice is advocated by two reasonings. First, a plate with several holes may be thought of as the zeroth-order approximation to a regularly perforated plate, where the energy is directly associated with

Keywords: plane elasticity problem, Kolosov–Muskhelishvili potentials, shape optimization, effective energy, extremal elastic structures, genetic algorithm.

The preliminary results of the paper were presented at the 7th EUROMECH Solid Mechanics Conference (ESMC2009), Lisbon, September 7–11, 2009.

the physically measurable effective moduli of the structure. Second, our previous experience shows that the energy minimization for a single hole [Vigdergauz 2006], and for two interacting holes [Vigdergauz 2008a], is not achieved at the expense of the boundary stresses. On the contrary, the energy-minimizing holes maintain a rather favourable stress distribution, with no excessive peaks; we may cautiously conclude that this is also the case here.

For concreteness, the plate is taken to be loaded by pure shear at infinity. This is more challenging than bulk load, which permits an analytical solution in many situations (*the equistress contours*, see, for instance: [Vigdergauz 2008a] and references therein).

Geometrically, the plane contains the main hole and, equally spaced on both sides of it, two identical unloading holes. The main hole is fixed as either a circle or as a slightly rounded square, which, in absence of auxiliary holes, provides the minimally possible energy under remote shear [Vigdergauz and Cherkaev 1986]. Our aim is, at a given inter-distance, to identify the shape and the area of the side holes that will minimize the hole-induced energy increment. Determining the minimum for such a solid and characterizing the associated extremal structures is an important problem, which arises in homogenization of composites and in optimal design.

Compared to the earlier optimization problem for two identical holes, the arrangement at hand has two complicating features. First, the boundary is partially fixed, since only the shapes of the side holes are changing, and, second, the area of the holes is also optimized. Both features are in contrast to the two-holes geometry fully described (up to scaling) by a single dimensionless parameter, which is the ratio of the hole area to the squared distance between the holes. Nevertheless, both new properties are treated here by enhancing the same numerical framework that was developed for the two holes case. The essential points of this framework can be described in terms of a numerical optimization strategy, where a direct problem solver is repeated many times in a searching space, until a pre-set convergence criterion is reached.

Here, the solver uses complex-valued Kolosov–Muskhelishvili (KM) potentials [Muskhelishvili 1975], which are obtained from a specially derived system of linear algebraic equations involving no singularities and, hence, providing a fast and accurate assessment of each possible hole shape, as was shown previously in a similar context [Vigdergauz 2008a]. A standardly configured genetic algorithm (GA) then employs the above-described solver for fitness evaluation in a gradientless search of the global optimum. Of importance here is the novel encoding scheme, where a shape is presented by a sequence of the first N Laurent coefficients of the function, mapping it conformally onto a unit circle. By adding one more design variable for the hole area, we transform each shape into a chromosome, concatenated of $(N+1)$ genes in the $(N+1)$-dimensional bounded searching space. The fixed central hole remains untouched, while a given distance between the holes is preserved by simply displacing the side hole decoded from a chromosome. This approach has proved to be rather advantageous for numerical solution of the problem at hand, both for a circular and for a square-like central hole.

The paper is organized as follows. For reader convenience, Section 2 summarizes the analytical basics required for further development. Section 3 presents, in terms of these tools, the exact problem formulation and describes the fast and stable direct solver for evaluation of the energy criterion at fixed holes' shapes. Section 4 describes the efficient and adaptive shape parametrization. Together, these three sections provide, to the maximum extent possible, the theoretical backbone for effective numerical simulations. Section 5 describes the features of genetic algorithm, designed specifically for the current

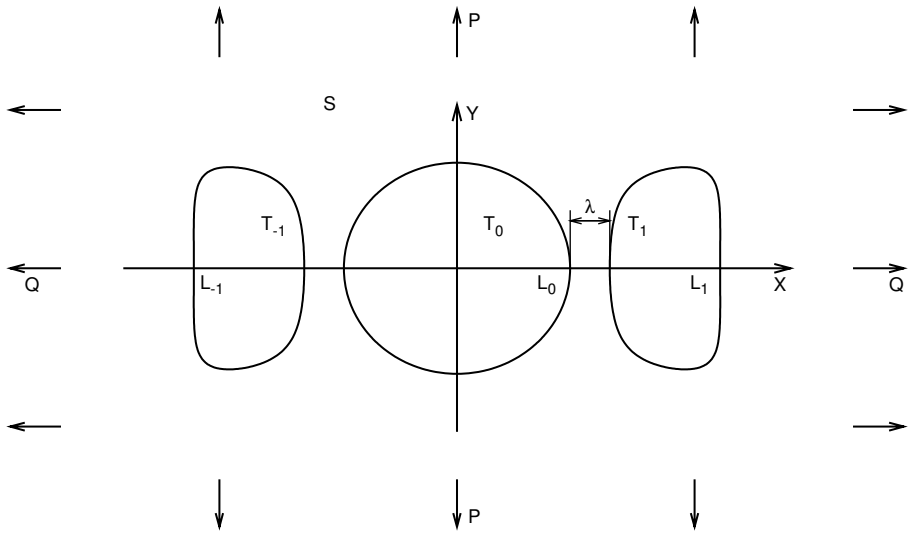

Figure 1. Problem schematic: an infinite plate with two identical holes under uniform stresses, cases $P = Q$ and $P = -Q$ correspond to remote bulk and shear, respectively. The piecewise smooth hole shape is symmetric about the x-axis and may have a finite number of angular points.

purposes. The numerical results are given at length in Section 6. Finally, Section 7 concludes the paper with a summary and remarks about future applications.

2. Analytical framework

Consider the setup in Figure 1, where a principal central hole T_0 in a thin elastic infinite plate interacts with two identical auxiliary holes T_{-1} and T_1, located symmetrically at a distance λ on each side of T_0. The areas of the holes are f_0 and $f_{-1} = f_1$, respectively. To fix the scale factor, we set $f_0 = \pi$.

For simplicity, the hole shapes L_j, $j = -1, 0, 1$, are traction-free, while the plate is remotely loaded by uniform nontangential stresses:

$$\sigma_{xx}^{\infty} = P, \quad \sigma_{yy}^{\infty} = Q, \quad \sigma_{xy}^{\infty} = 0. \tag{2-1}$$

The induced local stresses $\{\sigma_{xx}, \sigma_{yy}, \sigma_{xy}\}$ at any point $z = x + iy$ in the plate can be linearly expressed through a pair of complex-valued functions $\Phi_0(z)$ and $\Psi_0(z)$, holomorphic in the material-filled unbounded region S [Muskhelishvili 1975]:

$$\begin{aligned} \sigma_{xx}(z) + \sigma_{yy}(z) &= 4\,\mathrm{Re}\,\Phi_0(z), \\ \sigma_{yy}(z) - \sigma_{xx}(z) + 2i\sigma_{xy}(z) &= 2\big(\bar{z}\Phi_0'(z) + \Psi_0(z)\big). \end{aligned} \tag{2-2}$$

On account of symmetry, the potentials $\Phi_0(z)$, $\Psi_0(z)$ [Muskhelishvili 1975] are even functions of z:

$$\Phi_0(-z) = \Phi_0(z), \quad \Psi_0(-z) = \Psi_0(z) \qquad \text{for } z \in S, \tag{2-3}$$

with the asymptotics

$$\Phi_0(z) = B + \Phi(z), \quad \Psi_0(z) = \Gamma + \Psi(z) \qquad \text{with } \begin{cases} \Phi(z),\, \Psi(z) = O(|z|^{-2}) \ \text{ as } z \to \infty, \\ 4B = P + Q, \quad 2\Gamma = Q - P. \end{cases} \tag{2-4}$$

Hence, these potentials possess the following Laurent expansions [Alfors 1979], with purely real coefficients:

$$\Phi_0(z) - B = \Phi(z) = \sum_{k=2}^{\infty} \big(a_0^{(k)} \xi_k(z, 0) + a_1^{(k)} \xi_k(z, c)\big), \tag{2-5a}$$

$$\Psi_0(z) - \Gamma = \Psi(z) = \sum_{k=2}^{\infty} \big(b_0^{(k)} \xi_k(z, 0) + b_1^{(k)} \xi_k(z, c)\big), \tag{2-5b}$$

$$\xi_k(z, c) \equiv \frac{1}{(z-c)^k} + \frac{(-1)^k}{(z+c)^k}, \quad \xi_k(z, c) = \xi_k(-z, c) \quad \text{for } z \in S, \tag{2-5c}$$

$$\xi_k(z, 0) = \frac{2}{z^k} \ \text{ for } k = 2, 4, \ldots, \quad \xi_{2k+1}(z, 0) = 0 \ \text{ for } k = 3, 5, \ldots, \tag{2-5d}$$

where c is a fixed point on the X-axis inside the hole L_1.

It should be noted that only the first coefficients in (2-5a) and (2-5b) define the stress energy increment Δw brought by the holes into a given outer stress field (2-1) [Muskhelishvili 1975]:

$$\Delta w = 2\pi \big(2\Gamma_0 (a_0^{(2)} + 2a_1^{(2)}) + B_0 (b_0^{(2)} + 2b_1^{(2)})\big) E^{-1}, \tag{2-6}$$

where E is the Young modulus of the plate. This is in clear contrast to the local stresses (2-2), which involve all the coefficients (2-5a). This difference provides a great computational advantage.

The increment is a strictly positive definite bilinear form of B, Γ [Muskhelishvili 1975]:

$$\Delta w = B^2 \omega_{11} + 2B\Gamma \omega_{12} + \Gamma^2 \omega_{22} > 0 \quad \Longrightarrow \quad \omega_{11},\ \omega_{22} > 0,\ \omega_{11}\omega_{22} > \omega_{12}^2 \tag{2-7}$$

and depends on all the parameters involved in the problem. For future convenience, we normalize Δw by the total holes area $(\pi + 2f_1)$ and by E,

$$\Delta w = E\Delta w/(\pi + 2f_1) = B^2 w_{11} + 2B\Gamma w_{12} + \Gamma^2 w_{22}, \tag{2-8a}$$

$$w_{ij} = w_{ij}(L_0, L_1, \lambda, f_1) \quad \text{for } i, j = 1, 2,\ i \le j. \tag{2-8b}$$

Finally, the traction-free condition links the potentials along the holes' boundaries, in the following form:

$$2\frac{\partial \bar{t}}{\partial t} \operatorname{Re} \Phi(t) + \bar{t}\, \Phi'(t) + \Psi(t) = -2B \frac{\partial \bar{t}}{\partial t} - \Gamma, \quad t \in L; \quad L = L_{-1} + L_0 + L_1; \tag{2-9}$$

see [Muskhelishvili 1975], observing that identity (2-9) is specifically rearranged for future use.

Though mathematically simple, the increment Δw can be obtained only by finding the stress state in the plate at a given geometry. Using (2-2), this full-size direct elastostatic problem is equivalently replaced by the uniquely solved boundary value problem (2-9)+(2-4)+(2-1) in $\Phi_0(z)$ and $\Psi_0(z)$; see again [Muskhelishvili 1975]. It can be solved numerically, amongst many other possibilities, by substituting

the expansions (2-5) into (2-9), to arrive at an infinite system of algebraic equations in vector $\{x\}$ of the unknown Laurent coefficients:

$$\sum_{j=1}^{\infty} p_{ij} x_j = q_i \quad \text{for } i = 1, 2, \ldots. \tag{2-10}$$

The system matrix, $\{p_{ij}\}$, and the right hand side, $\{q_i\}$, are obtained by integrating specific combinations of the power terms and their conjugates in (2-5) over the boundaries of the holes. Analytically, this is a difficult problem, highly dependent on specific geometry, because only a circle $\{t : |t - c| = r\}$, that is,

$$(\bar{t} - \bar{c}) = r^2 (t - c)^{-1}, \tag{2-11}$$

possesses the simple relations between shape points t and $\bar{t}$ used for reducing the integrals to a closed form. Otherwise, numerical methods are called for. In a similar context we have proposed in [Vigdergauz 2006; 2008a] a fast and stable computational scheme employing the special parametric shape representation, as detailed in the next section.

3. Problem formulation and fast direct solver

Our aim now is to use the scheme sketched above as an inner solver, within the following optimization problem:

Given a central hole L_0 at an inter-distance λ from its neighbors, and given a far stress field, B, Γ, find the shape L_1 and the area f_1 of the Δw-optimal auxiliary holes, on which

$$\Delta w(B, \Gamma, L_0, L_1, \lambda, f_1) \xrightarrow[\{L_1\},\quad f_1 \le f]{} \min(B, \Gamma, L_0, \lambda), \tag{3-1}$$

where $\{L_1\}$ denotes the set of all closed curves with area less than a specified constant f. The curves are to have no cusps and no self-intersections.

The variable hole area is a rather novel feature in shape optimization in elasticity. This additional degree of freedom may provide certain advantages in minimizing the criterion (3-1). To be more specific, we suppose that the auxiliary holes may not be larger than the principal one,

$$f_1 \le f = f_0 = \pi. \tag{3-2}$$

Preparatory to solving the optimization problem (3-1), we prove the following elementary assertion:

Let the functions $f_1(z)$, $f_2(z)$ be holomorphic in the same domain D of the complex plane z. Also, let them be equal in all their derivatives at some interior point $z_0 \in D$:

$$f_1^{(k)}(z_0) = f_2^{(k)}(z_0) \qquad \text{for } k = 0, 1, \ldots. \tag{3-3}$$

Then both functions coincide identically throughout their common region of analyticity:

$$f_1(z) = f_2(z) \qquad \text{for all } z \in D. \tag{3-4}$$

Indeed, a holomorphic function is represented in a sufficiently small neighborhood of any interior point by a Taylor series [Alfors 1979]:

$$f_j(z) = c_{j,0} + c_{j,1}(z - z_0) + c_{j,2}(z - z_0)^2 + \cdots \quad \text{for } z, z_0 \in D \text{ with } \|z - z_0\| \le r_j, \tag{3-5}$$

where $j = 1, 2$. Considering (3-5) in $\|z - z_0\| \le \min(r_1, r_2)$, we conclude, in view of (3-3), that both Taylor series are the same: $c_{1,k} = c_{2,k}$ for $k = 0, 1, \ldots$, and, hence,

$$f_1(z) \equiv f_2(z) \quad \text{if } \|z - z_0\| \le \min(r_1, r_2). \tag{3-6}$$

The extended identity (3-4) now follows from (3-6) by the principle of analytical continuation [Alfors 1979].

Next, as in [Vigdergauz 2008a], we specifically employ the loading boundary condition (2-9). Integration of the both sides with the Cauchy kernel $dt/(t - z)$ over the holes' boundaries L gives

$$2\int_L \frac{\operatorname{Re}\Phi(t)\,d\bar{t}}{t-z} + \int_L \frac{\bar{t}\,\Phi'(t)\,dt}{t-z} + \int_L \frac{\Psi(t)\,dt}{t-z} = -2B\int_L \frac{d\bar{t}}{t-z} - \Gamma\int_L \frac{dt}{t-z}. \tag{3-7}$$

Inside either of the holes, each item in (3-7) represents a holomorphic function of z [Muskhelishvili 1975]. It is crucial for further derivations that the last left integral identically disappears, since its integrand $\Psi(t)$ is the boundary value of a holomorphic function *outside* the holes and vanishes at infinity [Alfors 1979]. In addition, the symmetry relations (2-3) allow for replacing the integral path L_{-1} with L_1, while the second right integral is simply $2\pi i\Gamma$, by the residue theorem. By virtue of all of the above, (3-7) is rewritten, after routine algebra, as

$$2\int_{L_0} \frac{\operatorname{Re}\Phi(t)\,d\bar{t}}{t-z} + \int_{L_0} \frac{\bar{t}\,\Phi'(t)\,dt}{t-z} + 2\int_{L_1} \operatorname{Re}\Phi(t)\eta_1(t,z)\,d\bar{t} + \int_{L_1} \bar{t}\,\Phi'(t)\eta_1(t,z)\,dt$$
$$= 2B\int_{L_0} \frac{d\bar{t}}{t-z} + \int_{L_1} \eta_1(t,z)\,d\bar{t} + 2\pi i\Gamma, \tag{3-8}$$

where $\eta_1(t, z)$ is defined similarly to (2-5c):

$$\eta_1(t,z) \equiv \frac{1}{t-z} + \frac{1}{t+z}, \quad \eta_1(t,-z) = \eta_1(t,z) \quad \text{for } z \in L_0, L_1. \tag{3-9}$$

The most common way of further transforming identity (3-7) is to obtain an equivalent *singular* integral equation, where z tends from the inside of the holes to their boundary $L_0 + L_1$ [Muskhelishvili 1975]. Alternatively, we employ (3-3)+(3-4) to equivalently recast (3-8) into a set of *regular* identities at $z_0 = c$:

$$2\int_{L_0} \frac{\operatorname{Re}\Phi(t)\,d\bar{t}}{(t-c)^k} + \int_{L_0} \frac{\bar{t}\,\Phi'(t)\,dt}{(t-c)^k} + 2\int_{L_1} \operatorname{Re}\Phi(t)\eta_k(t,c)\,d\bar{t} + \int_{L_1} \bar{t}\,\Phi'(t)\eta_k(t,c)\,dt$$
$$= 2B\int_{L_0} \frac{d\bar{t}}{(t-c)^k} + 2B\int_{L_1} \eta_k(t,c)\,d\bar{t} + 2\pi i\Gamma\delta_{k,1}, \tag{3-10}$$

and at $z_0 = 0$:

$$2\int_{L_0} \frac{\operatorname{Re}\Phi(t)\,d\bar{t}}{t^k} + \int_{L_0} \frac{\bar{t}\,\Phi'(t)\,dt}{t^k} + 2\int_{L_1} \operatorname{Re}\Phi(t)\eta_k(t,0)\,d\bar{t} + \int_{L_1} \bar{t}\,\Phi'(t)\eta_k(t,0)\,dt$$
$$= 2B\int_{L_0} \frac{d\bar{t}}{t^k} + 2B\int_{L_1} \eta_k(t,0)\,d\bar{t} + 2\pi i\Gamma\delta_{k,1}. \tag{3-11}$$

Here $\delta_{k,1}$ is the Kronecker delta and we have set, for $k = 0, 1, 2 \ldots$,

$$\eta_{k+1}(t,c) \equiv \frac{1}{(k)!}\frac{\partial^k \eta_1(t,z)}{\partial z^k}\bigg|_{z=c} = \frac{1}{(t-c)^{k+1}} + \frac{(-1)^k}{(t+c)^{k+1}}; \tag{3-12}$$

in particular, $\eta_{2k+1}(t,0) = 2/t^{2k+1}$ and $\eta_{2k+2}(t,0) = 0$. As prescribed by the symmetry of the problem, the kernels ξ_k and η_{k+1} differ in the sign of their second term.

Finally, substitution of the Laurent expansion (2-5) transforms (3-10)+(3-11) into the linear system (2-10) in the unknowns $x_{2k-1} = a_1^{(k)}$, $x_{2k} = a_0^{(2k)}$, $k = 1, 2, \ldots$

$$\begin{aligned}
p_{2k-1,2l-1} &= 2\int_{L_0+L_1} \operatorname{Re}\xi_{l+1}(t,c)\eta_k(t,c)\,d\bar{t} \qquad + \int_{L_0+L_1} \bar{t}\xi'_{l+1}(t,c)\eta_k(t,c)\,dt,\\
p_{2k-1,2l} &= 2\int_{L_0+L_1} \operatorname{Re}\xi_{2l-1}(t,0)\eta_k(t,c)(t,c)\,d\bar{t} + \int_{L_0+L_1} \bar{t}\xi'_{2l-1}(t,0)\eta_k(t,c)\,dt,\\
p_{2k,2l-1} &= 2\int_{L_0+L_1} \operatorname{Re}\xi_{l+1}(t,c)\eta_{2k-2}(t,0)\,d\bar{t} \quad + \int_{L_0+L_1} \bar{t}\xi'_{l+1}(t,c)\eta_{2k-2}(t,0)\,dt,\\
p_{2k,2l} &= 2\int_{L_0+L_1} \operatorname{Re}\xi_{2l-1}(t,0)\eta_{2k-2}(t,0)\,d\bar{t} \quad + \int_{L_0+L_1} \bar{t}\xi'_{2l-1}(t,0)\eta_{2k-2}(t,0)\,dt,\\
q_{2k-1} &= -2B\int_{L_0+L_1} d\bar{t}\eta_k(t,c) + \Gamma\delta_{k,1},\\
q_{2k} &= -2B\int_{L_0+L_1} d\bar{t}\eta_e t a_{2k-2}(t,0) + \Gamma\delta_{k,1}.
\end{aligned} \tag{3-13}$$

The kernels $\xi_k(t,c)$, $\xi_k(t,c)$, $\eta_k(t,c)$, $\eta_k(t,0)$ and, hence, the above integrals are regular. All entries in (3-13) are divided by $2\pi i$. Again, along circular shapes (2-11) they take a closed, though cumbersome, typical form of binomial coefficients and powers of c.

Remarkably, the resolving system (3-13) involves no Laurent coefficients $b_1^{(k)}, b_0^{(2k)}$ of $\Psi(z)$. Once the system is solved, they can be found by directly integrating the boundary condition (2-9),

$$2\pi i b_1^{(k)} = \int_{L_1} (t-c)^{2k-1} \operatorname{Re}\Phi(t)\,d\bar{t} + \int_{L_1} (t-c)^{2k-1}\bar{t}\,\Phi'(t)\,dt, \tag{3-14a}$$

$$2\pi i b_0^{(2k)} = \int_{L_0} t^{2k-1} \operatorname{Re}\Phi(t)\,d\bar{t} + \int_{L_0} t^{2k-1}\bar{t}\,\Phi'(t)\,dt. \tag{3-14b}$$

This halves the computational efforts compared to the commonly used approaches, where both potentials are solved simultaneously rather than in tandem.

4. Shape parametrization scheme

We are now in a position to enhance the proposed sequential solution of KM potentials by a numerical scheme for effectively evaluating the contour integrals (3-13). Within the optimization framework, this raises the question of how to validly encode an arbitrary hole. The commonly used discretization with nodal points is computationally expensive, due to their double use as design variables and as integration points. For reasonably accurate results, one should keep a needlessly large number of nodes, thus causing a dramatic slowdown of the optimization convergence.

In a similar, though more simple, context of free-boundary problems for a single elastic inclusion [Vigdergauz 2006], and for two identical holes [Vigdergauz 2008a], we devised an alternative shape parametrization scheme, which can also be used for the current purposes. For reader's convenience we briefly summarize this latter paper's approach, in which the design variables are *separated* from the integration points.

For this purpose, we narrow our focus to smooth closed curves L_1 that can be conformally mapped onto the unit circle $\gamma = \{\tau = e^{i\theta} : 0 \le \theta \le 2\pi\}$, by means of an analytic function $\Omega(t)$ with a small number N of initial nonzero Laurent terms [Alfors 1979]:

$$t \equiv \Omega(\tau) = \tau + \sum_{j=1}^{N} d_j \tau^{-j} \quad \text{with } t \in L_1,\ \tau \in \gamma \tag{4-1}$$

(note that $\tau^{-1} = \overline{\tau}$). The area of the region enclosed by L_1 is then

$$F_N = \pi\left(1 - \sum_{j=1}^{N} j|d_j|^2\right). \tag{4-2}$$

Thus, the novel feature of varying the area is realized simply by scaling the hole with the factor

$$f_1/F_N, \quad f_1 \le f. \tag{4-3}$$

It is quite significant that, in contrast to common practice, neither the elastic domain nor the stress-strain equations are really transformed. The mapping is used for the purely geometrical purpose of effectively presenting the searched shapes. Put otherwise, the novel shape representation involves a conformal mapping of a *single hole*, rather than of *all holes simultaneously*. This feature is especially useful for the partially fixed boundary, where the major hole simply remains unmapped.

Taken in this case as design variables, the mapping coefficients have the following substantial advantages over the nodal points representation:

- They are naturally ordered, in the sense that the higher the coefficient, the smaller its global impact on the inclusion shape. Indeed, geometrically, the high-order mapping coefficients are responsible mainly for forming large curvature isolated shape points and, thus, have little effect on the *integral*-type energy increment Δw. In practice, this provides a rapid convergence to the global optimum at small values of N (typically, $N \le 7$, as shown in Section 6). This convenience disappears for the problem of minimizing the *local* stresses, where N should be sufficiently large to accurately compute possible stress concentration at large curvature points. For this reason, the stress optimization remains beyond the current scope.
- They fall into the successfully narrowing intervals,

$$-\frac{1}{\sqrt{j}} \le d_j \le \frac{1}{\sqrt{j}} \quad \text{for } j = 1, 2, \ldots, \tag{4-4}$$

  as a result of the uniqueness of conformal mapping [Alfors 1979]. This allows us to treat these intervals and the two-sided inequality (3-2) for the noncentral hole area as linear constraints in the optimization problem (3-1), which is reformulated in the following manner:

For a given finite number N of mapping coefficients and fixing the other parameters involved in (3-1)*, find the energy-minimizing shape and area of the auxiliary hole* L_1*,*

$$\Delta\omega(B, \Gamma, L_0, L_1, \lambda, f_1) \xrightarrow[\{L_1\}_N, \quad f_1 \le f]{} \min_N(B, \Gamma, L_0, \lambda). \tag{4-5}$$

Put differently, we simplify the initial shape optimization problem by replacing the comprehensive pool $\{L_1\}$ of all admissible curves by its N-mapped subset

$$\left\{\{L_1\}_N : \{L_1\}_N \subset \{L_1\},\ \min_N(B, \Gamma, L_0, \lambda) \ge \min(B, \Gamma, L_0, \lambda).\right\}$$

By taking the differential of (4-1) and its conjugate, and using the identity (2-11), we get

$$dt = \Omega'(\tau)\, d\tau = i\left(\tau - \sum_{j=1}^{N} j d_j \tau^{-j}\right) d\theta, \quad d\bar{t} = -i\left(\tau^{-1} - \sum_{j=1}^{N} j d_j \tau^{j}\right) d\theta. \tag{4-6}$$

Any integration path $L_1 \in \{L_1\}_N$ in (3-13) is transformed to the unit circumference γ, independently of the design variables $\{d_1, d_2, \ldots, d_N\}$. The resultant regular integrals along γ can be evaluated by any appropriate numerical scheme. We employ the standard Gaussian quadrature rule with N_p equally spaced points. The design variables here are fully separated from the integration points.

Our experience suggests that the reformulation (4-5) of the optimization problem is well suited to be solved by the genetic algorithm (GA).

5. GA scheme: related results and current specifics

Devised by Holland [1975], the genetic algorithm (GA) exploits the heuristic that simulates natural evolution processes, such as selection and mutation. It evolves candidate solutions for problems that have large solution space and are not amenable to exhaustive search or traditional optimization techniques.

Typically, GA starts with a random population of encoded candidate solutions, called chromosomes. Then the fitness of each candidate solution in the current population is evaluated to select the fittest candidate solutions as parents of the next generation of candidate solutions. After being selected for reproduction, parents are recombined (using a crossover operator) and mutated (using a mutation operator) to generate offspring. The fittest parents and the new offsprings form a new population, for which the process is repeated to create new populations.

As applied to the problem at hand, the GA operators are specified in the following way:

Each chromosome concatenates $N+1$ two-byte integers I_j in the range $-M \le I_j \le M$ where $M = 2^{15} - 1$ and $j = 0, 1, \ldots, N$. In view of (3-2), (4-4), and (4-3) the chromosomes encode a possible shape $L_1 \in \{L_1\}_N$ through its area and its Laurent coefficients:

$$f_1 = (1 + I_0/M)\, f/2, \tag{5-1a}$$

$$d_j = I_j/M\big/\sqrt{j} \quad \text{for } j = 1, 2 \ldots, N. \tag{5-1b}$$

Substitution of (5-1) into (4-1) decodes the corresponding shape. However, self-intersecting shapes may appear, since the inequalities (4-4) are only necessary, not sufficient, to guarantee their absence. To our knowledge, no conditions on the coefficients d_j are known which trim out only self-intersecting curves.

Therefore, we check each decoded curve for possibly breaking monotonicity, demanding that

$$\frac{d \arg \Omega(\tau)}{d\theta} \geq 0 \quad \text{for } 0 \leq \theta \leq 2\pi; \tag{5-2}$$

this corresponds to the more restrictive shape property of star-shapeness. Physically, it is clear anyway that only star-shaped holes are promising for optimization. In the numerical simulations (Section 6) this is attested to by the fact that the optimal values of d_j, $j = 1, 2, \ldots, N$, are rather distant from the limiting values in (4-4).

Inequality (5-2) is verified at each integration point along the unit circle $\gamma : |\tau| = 1$. Wherever (5-2) is violated, the corresponding shape obtains a penalty as its fitness, and the GA process takes the next candidate. The idea is to assign the penalty by measuring the squared violation and multiplying it by a very large constant. A shape allowed by (5-2) is further scaled with respect to (5-1b) and is displaced from the origin at the distance

$$c = \lambda + \min\big(\operatorname{Re} L_0(x, y) - \operatorname{Re} L_1(x, y)\big), \tag{5-3}$$

to satisfy the given geometry. The displacement value c from (5-3) serves as the parameter in (3-13) and in all the relative transformations. After that, the fitness of a feasible candidate is evaluated by (1) solving first the system (3-13) truncated to size $K \times K$; (2) restoring the second potential $\Psi(z)$ by use of (3-14); and (3) substituting the first few Laurent coefficients into the resulting expression (2-6) for the energy increment. Step (1) is the most time-consuming phase of GA; hence, all the economy reasoning should be applied here. First, due to symmetry, the system is pure real. Second, the coefficients $b_0^{(2)}$, $b_1^{(2)}$

GA parameter	Parameter value(s)
Gene	Integer in $[-32767; 32767]$
Individual	Interface shape
Population size	1000–25000, depending on inter-distance
Number of genes, $N + 1$	up to 8
Initial population	1000–25000 random individuals
Selection	Tournament
Elitism	Four best individuals
Crossover	1-point
Crossover rate	0.99
Creep mutation	By randomly changing a bit
Creep mutation rate	0.35
Jump mutation	By adding a random integer, typically in the range $[-4; 4]$
Jump mutation rate	0.35
Stopping criterion	After M iterations, M in the range [100; 150]
Resolving system size	$K = 36$
Number of integration points	$N_p = 720$ (in the interval $[0, \pi]$)

Table 1. GA operator types, their probability rates and related parameters typically used in further optimizations.

of $\Psi(z)$ disappear from the energy increment (2-6) when the remote load is pure shear ($B = 0$). This allows for avoiding step (2) calculations and for truncating the system (3-13) at relatively moderate size, since only the two first unknowns, $a_0^{(2)}$ and $a_1^{(2)}$, define the increment (2-6). Namely, in such a way a single energy minimizing hole [Vigdergauz 2006] and two interacting holes [Vigdergauz 2008a] were identified earlier. In the first case, additionally, the unknowns partly vanish due to four-fold symmetry, while the equations (3-13) acquire a finite-difference form [Levy and Lessman 1959] that is resolved analytically, with no truncation.

The main result so obtained in [Vigdergauz 2006] is that the energy-minimizing singular hole under remote shear L_* looks like a square with slightly rounded corners, and provides the global increment minimum

$$\Delta w_{22}(0, 1, \lambda, L_*) \approx 0.928623, \tag{5-4}$$

which is somewhat less than the value for a circle γ [Muskhelishvili 1975],

$$\Delta w_{22}(0, 1, \lambda, \gamma) = 1.00. \tag{5-5}$$

In what follows, we also suppose that the plate is subject to pure shear at infinity, using both values (5-4) and (5-5) for future comparison. An immediate conclusion can be drawn here about the behavior of the corresponding increment (2-8), when the inter-distance λ tends to infinity. In this case, the resultant energy is simply a weighted sum of the energies (5-4) and (5-5) with the optimized side holes nearing L_*. Therefore, we have

$$\min_{\{L_1\}} \lim_{\lambda\to\infty} w_{22} = \min_{\{f_1 \le f_0\}} w_{22}(L_0, L_*, f_1) \tag{5-6}$$

$$= \begin{cases} \min\limits_{\{f_1 \le f_0\}} \dfrac{f_0 + 2\times 0.928623 f_1}{f_0 + 2f_1} = 0.952416 \text{ (achieved for } f_1 = f_0) & \text{when } L_0 = \gamma, \\ \min\limits_{\{f_1 \le f_0\}} \dfrac{0.928623(f_0 + 2f_1)}{f_0 + 2f_1} = 0.928623 \text{ (achieved for any } f_0, f_1) & \text{when } L_0 = L_*. \end{cases}$$

It is worthy of note that, when f_1 tends to infinity, the upper expression in (5-6) is a decreasing function of f_1 everywhere in the interval $0 \le f_1 < \infty$, with the limit (5-4). Therefore, in the absence of the inequality constraint (3-2), the optimized hole area grows infinitely large with the distance, as observed in numerical simulations. The lower expression, naturally, is independent of the areas f_0, f_1, and assumes the constant value (5-4).

Though many schemes are suggested to enhance GA, the relatively small number N of design variables allows us to use a rather simple configuration, with a number of heuristic parameters. For achieving better efficiency, these need to be adjusted by preliminary numerical tests for assessing the GA's stability and convergence speed. Table 1 on the previous page gives the chosen values of the parameters.

6. Numerical results

A wide set of GA-based simulations was performed to numerically solve the optimization problem (4-5) in the representative inter-distance interval $0.2 \le \lambda \le 5.0$. To ensure the accuracy of the results, all output data were computed several times, randomly starting each GA process and stopping it after a rather large number M of iterations, when there is no more variation of the results. At a fixed inter-distance λ, the computed minimum w_{22} depends on both N and M, and should converge separately with increase of

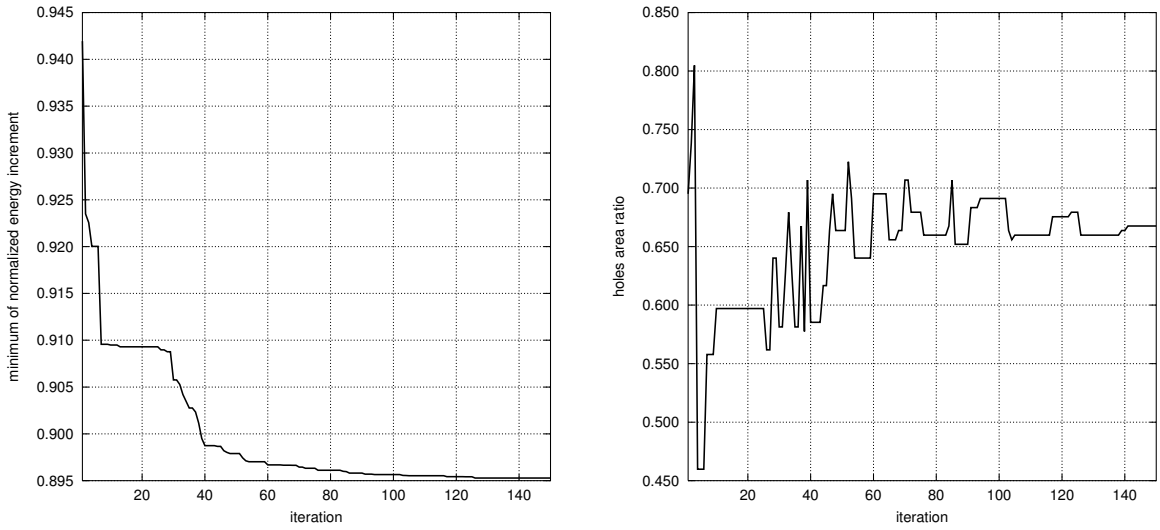

Figure 2. Hole shape identification: progress of a typical genetic optimization run with increasing M for the energy increment (left) and for the side hole area (right).

either of them. A typical iteration convergence for the GA scheme is shown in Figure 2. The convergence to the global optimum with increasing number N of mapping terms was assessed by the relative proximity of the optimal values for the first successive values of N, as shown in Table 2, at the hard-to-compute value $\lambda = 0.2$. The evolution of the optimized shape with M and N is presented in Figure 3. The right part of the figure illustrates the fact, already noted, that the higher mapping coefficients change the optimized shape only locally.

The remaining results are displayed in parallel for the circular and the square-like central hole. The most labor-intensive is Figure 4, which demonstrate the dependence of the energy increment minimum

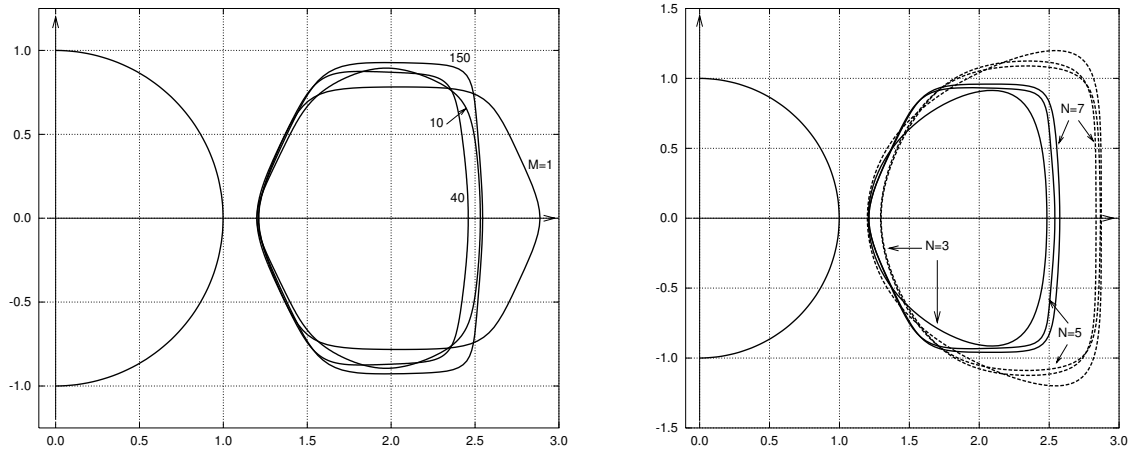

Figure 3. Hole shape identification: progress of a typical genetic optimization run at $\lambda = 0.2$ with M (left) and with N (right). The dashed lines show the optimal shapes at the fixed side hole area $f_1 = f_0$.

N	d_1	d_2	d_3	d_4	d_5	d_6	d_7	f_1/f_0	$\min \delta w_{22}$
1	−0.2039							0.3892	0.9367
2	−0.1843	−0.0804						0.5539	0.9204
3	−0.1686	−0.0902	−0.0144					0,5892	0.9200
4	−0.1804	−0.0412	−0.0118	−0.0343				0.5931	0.9113
5	−0.1863	−0.0627	−0.0484	−0.0284	0.0282			0.6990	0.8963
6	−0.1863	−0.0627	−0.0484	−0.0284	0.0282	0.0000		0.6990	0.8963
7	−0.1843	−0.0627	−0.0497	−0.0314	0.0282	0.0026	0.0022	0.6873	0.8955

Table 2. Circular central hole case: optimal mapping coefficients for the side hole and the corresponding min Δw_{22} for different values of N.

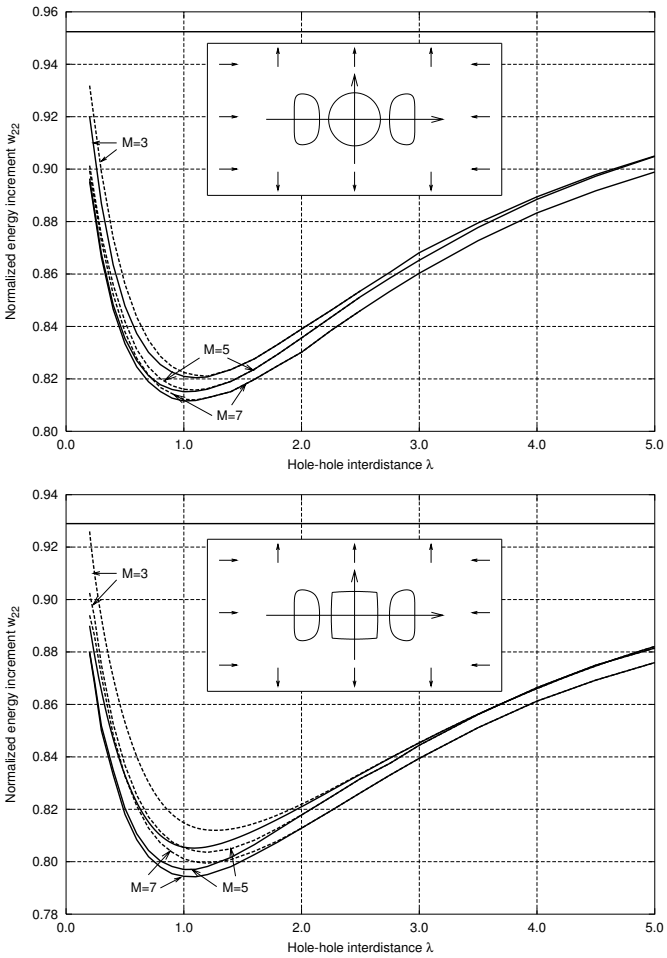

Figure 4. Values of min w_{22} as a function of the inter-distance λ with dependence on the problem mapping size N, with (solid lines) and without (dashed lines) optimization of the hole area. The value (5-6) of the minimum energy increment induced by the widely spaced holes is also added for comparison (straight line). Top: circular central hole case. Bottom: square-like central hole case.

w_{22} on the distance λ between the central and the side holes. Comparison to the limiting values (5-6) of the widely spaced optimal holes (straight lines) shows that the interaction of the holes provides an appreciable energy gain at any inter-distance λ, except at very small ones. Clear optima are observed in both cases for λ in the range 1.05–1.10, with a relative decrease in the energy of $\approx 15\%$, as compared to the values (5-6) for the corresponding case of the noninteracting holes. Compared to the increment (5-5) of a single circular hole, the auxiliary holes raise the gain to $\approx 19\%$, while a pair of identical interacting optimal holes conserves $\approx 12\%$ of the energy [Vigdergauz 2008a]. We note that the pre-optimization levels (5-4), (5-5), and, hence, the energy gain are both less for the square-like central hole. The difference between the solid and the dashed lines reflects the contribution related solely to the hole area variation in interval (5-1a), which remains small even near the global increment minimum. This indicates that the potential of changing the area of the hole for energy optimization is rather limited at the current geometry.

Figure 5 exhibits the shape evolution with the increasing distance λ. As expected, in both cases the optimal shape grades into the square-like optimal hole of the area $f_1 = f_0 = \pi$, in accordance with (5-6) and (3-2).

The dependence $f_1(\lambda)$ of the optimal hole area on the spacing between the holes is shown in Figure 6.

Finally, we try to qualitatively evaluate the hoop stresses induced along the energy optimal and the fixed central hole. When L_0 is a unit circle, the angular stress distribution obtained as a by-product of

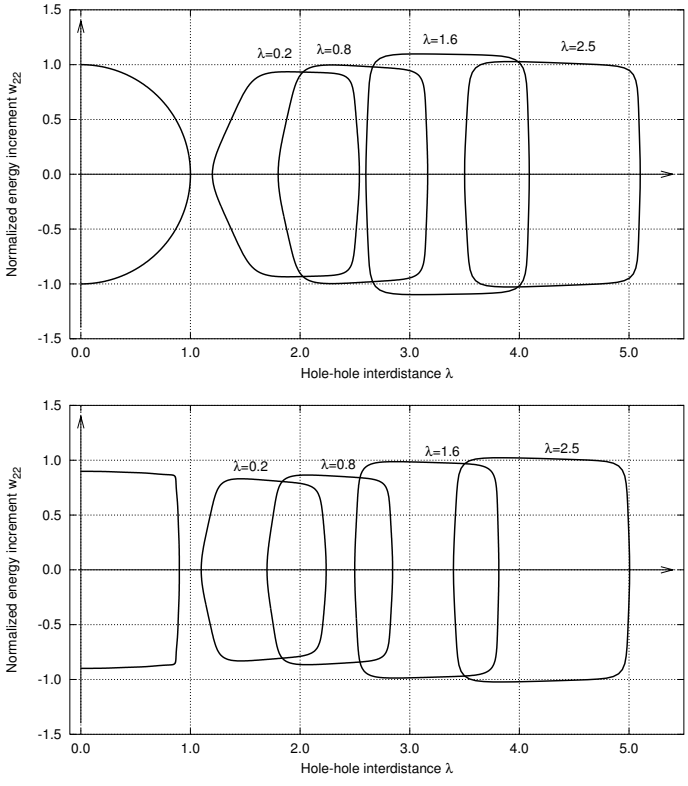

Figure 5. Evolution of the energy-minimizing hole with the distance d at $N = 7$, for the circular (top) and square-like (bottom) central hole.

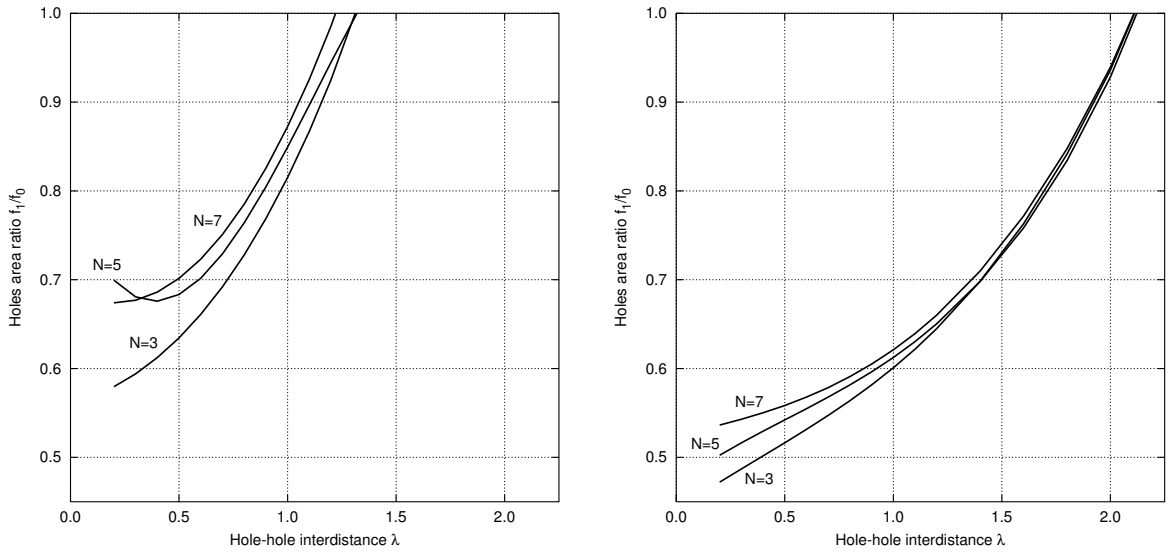

Figure 6. Ratio of the optimal and fixed hole areas as a function of their inter-distance for the circular (left) and the square-like (right) central hole.

the energy optimization is shown in Figure 7. The nonphysical oscillations observed indicate that the currently configured optimization scheme is not adequate for quantitative assessment of the stresses. On the other hand, the oscillations occur well away from the global extrema, so the latter can be cautiously used to conclude that, as N increases, the stresses maxima show a decrease (though not monotonic) in parallel with the energy (Table 3).

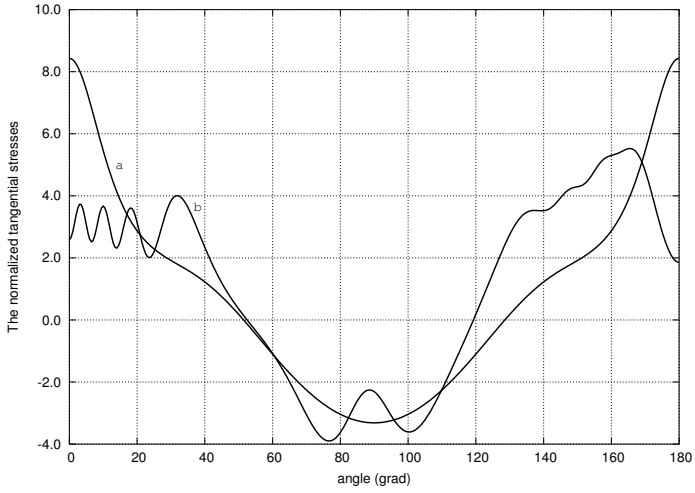

Figure 7. Circular central hole case: hoop stresses distribution along the central (a) and the energy-minimizing side holes (b), for $N = 7$ and $\lambda = 0.2$. The holes themselves are depicted in Figure 3, left.

	N	0	1	2	3	5	7
L_0	maximum	14.0200	9.6408	8.6397	9.2894	8.4561	8.4309
	minimum	−3.1456	−3.6886	−3,4341	−3.4155	−3.3545	−3.3145
L_1	maximum	11.0186	7.3296	6.6463	7.1169	5.6460	5.5241
	minimum	−6.2377	−3.9310	−4.2924	−4.2819	−3.9522	−3.9000

Table 3. Extremal values of the hoop stresses along the central circular and side energy-minimizing holes at $\lambda = 0.2$ with increasing number N of the mapping terms from $N = 0$ (a circle) and on.

7. Closure and future applications

The paper presented a GA-based study of a rather difficult shape optimization problem in an infinite 2D elastic region with partially fixed boundary. This was done by combining the complex variable technique with a novel shape representation specially tailored for the current purposes. For clarity, we repeat here the essential points of the approach.

First, the advanced direct solver is employed for a fast and stable fitness evaluation. The solver engine is based on a standard numerical treatment of a specially derived system of linear algebraic equations in Laurent coefficients for the first KM potential only. The system entries involve boundary integrals of a regular, rather than a singular, type.

Second, an efficient shape encoding scheme is used within the GA framework. Based on a separate conformal mapping of each free contour, it has a twofold benefit over the commonly used nodal points representation. First, as design variables, the mapping coefficients drastically reduce the computational size of the problem, because even a small number of them provides a representative pool of admissible curves. Possible excessive smoothing of angular points through neglecting the high-order coefficients is counteracted by the integral nature of the energy-related criterion. Second, any mutual arrangement of the mapped shapes is straightforwardly met by displacing and scaling.

The approach described works well also when elastic inclusions are taken instead of holes [Vigdergauz 2008b], and may be applied to similar problems in other fields of continuum mechanics. In elastostatics, it seems promising to use the proposed scheme for yet unsolved shape optimization problems in *finite* domains. We are now pursuing this issue.

References

[Alfors 1979] L. Alfors, *Complex analysis*, 3rd edition ed., McGraw-Hill, New York, 1979.

[Holland 1975] J. H. Holland, *Adaptation in natural and artificial systems*, University of Michigan Press, Ann Arbor, MI, 1975.

[Levy and Lessman 1959] H. Levy and F. Lessman, *Finite difference equations*, Pitman, London, 1959.

[Muskhelishvili 1975] N. I. Muskhelishvili, *Some basic problems of the mathematical theory of elasticity*, 2nd ed., Noordhoff, Leiden, 1975.

[Vigdergauz 2006] S. B. Vigdergauz, "Energy-minimizing hole in an elastic plate under remote shear", *J. Mech. Mater. Struct.* **1**:2 (2006), 387–406.

[Vigdergauz 2008a] S. B. Vigdergauz, "Shape optimization in an elastic plate under remote shear: from single to interacting holes", *J. Mech. Mater. Struct.* **3**:7 (2008), 1341–1363.

[Vigdergauz 2008b] S. B. Vigdergauz, "Stress-minimizing inclusion in an elastic plate under remote shear", *J. Mech. Mater. Struct.* **3**:1 (2008), 63–83.

[Vigdergauz and Cherkaev 1986] S. B. Vigdergauz and A. V. Cherkaev, "A hole in a plate optimal for its biaxial extension-compression", *J. Appl. Math. Mech.* **50**:3 (1986), 401–404.

Received 1 Aug 2009. Revised 26 Dec 2009. Accepted 28 Dec 2009.

SHMUEL VIGDERGAUZ: smuel@iec.co.il
Research and Development Division, The Israel Electric Corporation Ltd., P.O.Box 10, 31000 Haifa, Israel

JOURNAL OF MECHANICS OF MATERIALS AND STRUCTURES

http://www.jomms.org

Founded by Charles R. Steele and Marie-Louise Steele

Cover design: Alex Scorpan — Cover photo: Mando Gomez, www.mandolux.com

See inside back cover or http://www.jomms.org for submission guidelines.

JoMMS (ISSN 1559-3959) is published in 10 issues a year. The subscription price for 2010 is US $500/year for the electronic version, and $660/year (+$60 shipping outside the US) for print and electronic. Subscriptions, requests for back issues, and changes of address should be sent to Mathematical Sciences Publishers, Department of Mathematics, University of California, Berkeley, CA 94720–3840.

JoMMS peer-review and production is managed by EditFLOW™ from Mathematical Sciences Publishers.

PUBLISHED BY

mathematical sciences publishers

http://www.mathscipub.org

A NON-PROFIT CORPORATION

Typeset in LaTeX

Journal of Mechanics of Materials and Structures

Volume 5, No. 4 April 2010

1559-3959(2010)5:4;1-E